PONTIFICIA UNIVERSIDAD CATOLICA DE CHILE
SCHOOL OF ENGINEERING

OPTIMIZATION OF MRI ACQUISITION PARAMETERS USING VISUAL PERCEPTION INFORMATION

JAVIER JACOBSEN POHLENZ

Thesis submitted to the Office of Research and Graduate Studies
in partial fulfillment of the requirements for the degree of
Master of Science in Engineering

Advisor:
PABLO IRARRÁZAVAL M.

Santiago de Chile, January 2010

PONTIFICIA UNIVERSIDAD CATOLICA DE CHILE
SCHOOL OF ENGINEERING

OPTIMIZATION OF MRI ACQUISITION PARAMETERS USING VISUAL PERCEPTION INFORMATION

JAVIER JACOBSEN POHLENZ

Members of the Committee:
PABLO IRARRÁZAVAL M.
CRISTIÁN TEJOS
JAIME NAVÓN
ISIDRO HUETE

Thesis submitted to the Office of Research and Graduate Studies
in partial fulfillment of the requirements for the degree of
Master of Science in Engineering

Santiago de Chile, January 2010

A Romi, mi familia y amigos.

ACKNOWLEDGEMENTS

This research was made thanks to Conicyt through the grants Fondecyt 1070674, Fondecyt 1100529, Fondef D05I10358 and Proyecto Anillo PBCT-ACT-79.

I acknowledge Pablo Irarrázaval and Cristián Tejos, advisor and coadvisor of this research respectively, for their aid and their willingness to help me during the course of the research. I also acknowledge the other students and researchers of the Biomedical Imaging Center for their kindness and ideas during the meetings that were held at the Center.

I would also like to acknowledge Carlos, Agustin, Romi, Gonzalo, Álvaro, Ruby, Caro, Vicente, Cristóbal, Claudia and José Miguel, for their help and patience when I needed volunteers for MRIs. And Universidad Católica radiology residents for rating the images.

Finally, I acknowledge particularly Romi for her unconditional support, Carlos for making this stage more enjoyable, and my family for giving me this opportunity.

TABLE OF CONTENTS

LIST OF FIGURES

LIST OF TABLES

ABSTRACT

To define an MRI acquisition (protocol) is not trivial process due to the large number of parameters to be set. The visualization of structures of interest strongly depends on these parameters, which are selected manually and therefore requires vast experience from the operator.

There are some methods for optimizing these acquisition parameters, using cost functions derived from mathematical calculations of contrast between tissues of interest. These cost functions do not always correlate with the visual perception of the contrast, because they do not consider relevant features of the Human Visual System (HVS). Furthermore, they are not fully automatic since they require a prior manual segmentation of the tissues of interest.

We propose an automatic optimization method, using Visibility Maps based on HVS models. We consider two main properties of the HVS: sensitivity to spatial frequency and contrast.

The cost function of our optimization is an index obtained from the Visibility Maps, which allows maximizing the relevant information to the HVS contained in a region of interest.

We use our method to maximize the visibility of White Matter (WM) in an Inversion Recovery sequence, and the contrast between WM and Gray Matter in a Spin Echo sequence. The results show that our index can measure the visibility of the structures under study and the optimal parameter configuration found by our method outperforms existing methods and corresponds with the optimum found by experts.

Keywords: Magnetic Resonance Imaging, Human Visual System, Acquisition parameter optimization, quality assessment.

RESUMEN

La adquisión de imágenes de Resonancia Magnética no es un proceso trivial debido al gran número de parámetros que hay que definir. La visualización de estructuras de interés depende fuertemente de estos parámetros, los cuales son escogidos manualmente por lo cual se necesita una vasta experiencia en el uso del resonador.

Existen algunos métodos que han intentado optimizar los parámetros de adquisición utilizando funciones de costo obtenidas a partir de cálculos matemáticos de contraste entre los tejidos de interés. Estas funciones de costo no siempre tienen correspondencia con la percepción visual del contraste entre los tejidos, ya que no consideran aspectos relevantes del Sistema Visual Humano (HVS). Además, la optimización no es totalmente automática pues supone una previa segmentación manual de los tejidos de interés.

Nosotros proponemos un método de optimización automático, utilizando Mapas de Visibilidad basados en modelos del HVS. Consideramos dos propiedades fundamentales del HVS: la sensibilidad a frecuencias espaciales y al contraste.

La función de costo de nuestra optimización proviene de un índice que obtenemos de los Mapas de Visibilidad, el cual permite maximizar la información relevante al HVS contenida en una región de interés previamente definida.

Utilizamos nuestro método para maximizar la visibilidad de Materia Blanca (MB) en una secuencia Inversion Recovery, y la diferenciación entre MB y Materia Gris en una secuencia Spin Echo. Los resultados muestran que nuestro índice permite medir satisfactoriamente la visibilidad de las estructuras en estudio y que la configuración óptima de parámetros encontrada por nuestro método tiene correspondencia con el óptimo encontrado por expertos.

Palabras Claves: Resonancia Magnética, Sistema Visual Humano, Optimización de parámetros de adquisición, calidad de imágenes.

1. INTRODUCTION

Magnetic Resonance Imaging (MRI) has multiple degrees of freedom as there are many parameters that define the scan. The contrast or visualization of structures of interest (e.g. tumors, pathologies, tissues) highly depends on these parameters. The selection of them is always done heuristically and requires vast experience from the operator. Furthermore, sometimes it is not simple to predict the effect on the visibility of the structures of interest when a parameter is modified.

A few optimization methods have been published to automate or facilitate the parameter setting for different MRI applications such as tensor shapes and orientations in difussion-tensor imaging (DTI) (Hasan et al., 2002; Papadakis et al., 1999; Peng & Arfanakis, 2007; Lee et al., 2006; Skare et al., 2000; Jones et al., 1999), where the accuracy of the measurements depends on the gradient encoding scheme used. Other methods are focused on selecting optimal acquisition parameters using performance measures such as Signal to Noise Ratio or Contrast to Noise Ratio (Kim et al., 2006; Alger et al., 2001; Vidarsson et al., 2005; Dousset & al., 1989), where some MRI scans are obtained using different acquisition parameters. The signal intensities of the tissue of interest is then measured (using manual segmentation), subtracted and divided by the noise intensity to obtain the performance metric of each scan. When there exists an image that can be used as reference, the most common measure of quality is the Root Mean Square Error (RMSE) with respect to that image. It is easy to compute, it has a clear physical meaning, and it is convenient for optimization algorithms. Nevertheless, its disadvantages are widely recognized. The RMSE heavily penalizes differences that are irrelevant for the human observer.

We propose a Quality Assessment (QA) approach in which the acquisition parameters are defined as in an optimization problem. Importantly, the optimized cost function incorporates features of the Human Visual System (HVS). We evaluate this function by acquiring directly with the scanner image samples (a fragment of the field of view), computing an index of them, and fitting a parametric cost function to the samples. The goal is to find the MRI acquisition parameters that maximize the visibility of a desired structure, without the need of prior segmentation of images. We propose to compute a scalar index from Visibility Maps (VM) that measure the visibility of image features according to two perceptual criteria: the sensitivity of the HVS to different spatial frequencies and to different contrasts. The first one is related to the minimum contrast needed for an object to become visible for any given spatial frequency; and the second one is related to how the contrast sensitivity changes depending on the background intensity.

Image Quality Assessment is a challenge, although there are some indexes that correlate well with the subjective quality of the images, but they can not be used as a cost function to optimize the visibility of resonance images because they require prior information, such as a reference image, which is not available.

As measurement of quality we propose to use a scalar metric of the Visibility Maps (VM). In this work we introduce these maps which assign a visibility value to each pixel of the image. The visibility value, in turn depends on the spatial frequency and average intensity of the background. The advantage of this metric is that it does not require a reference image or a precise segmentation so that it is straightforward to obtain optimal acquisition parameters.

2. THEORY

In this section we present a brief description of the MRI acquisition process, we review existing quality metrics and present our proposal for a metric based on some HVS features.

2.1. Conceptualization of the MRI Acquisition

To perform an MR scan, the medical technologist acquires an image using previously defined parameters which are calculated based on historical data from other patients. Subsequently, the medical technologist observes the obtained image and decides whether a modification of the acquisition parameters is needed or not (as shown schematically in Figure 2.1). As a new acquisition is expensive, it is unusual to acquire more than twice, so the image obtained from the patient does not always correspond to the optimal, especially if it has some unusual structures.

Our proposal consists on replicating the acquisition process performed by the medical technologist but using a metric that considers some features of the HVS, so as to obtain automatically the optimal image of the patient.

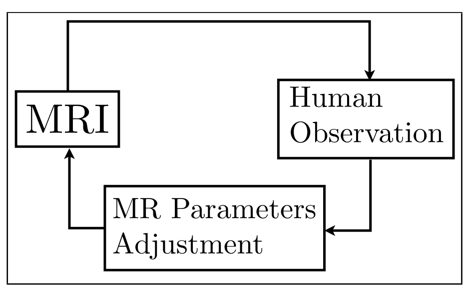

FIGURE 2.1. MRI parameters setting using human observation.

2.2. Existing Quality Metrics

Since our method can be thought as a quality assessment process, we now review the existing methods in this area.

The goal of quality assessment research is to design algorithms for objective evaluation in a way that can automatically predict perceptual image quality. Most of the proposed metrics require a reference image with "perfect" quality, which is used as a benchmark to assess the quality of a similar image. These methods, known as Full Reference Quality Assessment (FR QA), can be categorized into six groups according to the type of information they use (Avcibas et al., 2002).

(i) Pixel difference-based measures: Such as Peak Signal-to-Noise Ratio (PSNR) and Root Mean Squared Error (RMSE). These metrics are commonly used in medical images because of their simplicity, clear physical meaning and optimization convenience.

(ii) Correlation-based measures: They are calculated by the correlation of pixels. In this category are the Czekanowski coefficient (Czekanowski, 1913), Universal Quality Index (Z. Wang & Bovik, 2002) and SSIM (Z. Wang et al., 2004). The latter compares local patterns of pixel intensities which have been normalized in luminance and contrast in order to measure structural differences only. This index also has some adaptations, using HVS models (B. Wang et al., 2008), wavelet domain (Yang et al., 2008), multi-scale analysis (Z. Wang et al., 2003) and edge-based structural similarities (Chen et al., 2006).

(iii) Edge-based measures: These metrics quantify the displacement of edge positions or their consistency across resolution levels. Some examples of this category are the Pratt measure (Pratt, 1978), based on prior knowledge of the reference edge map, and the Edge Stability Measure (Carevic & Caelli, 1997), based on multi-resolution consistency of edge maps.

(iv) Spectral distance-based measures: They are based on Fourier magnitude and/or phase spectral discrepancy.

(v) Context-based measures: They penalize differences based on various functionals of the multidimensional context probability, like the Rate distortion measure, Hellinger distance and Spearman rank correlation (Spearman, 1987).

(vi) HVS-based measures: These metrics use HVS models to predict image quality. Some examples are: DCTune (Watson, 1993) which propose a luminance adaptation and masking effect model in edge regions; Zhang et al. (2005) propose a method based on *just noticeable differences* (JND) which allows the measurement of visual distortion and signal compression; Wavelet visible difference predictor (Bradley, 1999), which allows predicting visible differences between an image without distortion and noisy or compressed version of it, using the image wavelet domain; Chandler & Hemami (2007) propose a visual signal-to-noise ratio (VSNR) that takes into account low-level HVS properties of contrast sensitivity and visual masking; and finally, VIF (Sheikh & Bovik, 2006), which presents the QA problem as an *information fidelity problem* (quantify the loss of image information and explore the relationship between image information and visual quality) and approximates the HVS as a "distortion channel", in which the amount of information that can flow through it is restricted.

Pixel difference-based measures are commonly used as benchmark for their simplicity and low computational requirements, but often their results do not correspond to human perception of differences. Some studies (Sheikh et al., 2006; Ponomarenko et al., 2009; Chandler & Hemami, 2007) have shown good performance of Correlation-based measures and HVS-based measures, in particular SSIM, VIF and VSNR. However they can not be used to optimize the visualization of structures in MRI, since they require a reference image that is not available.

There are some metrics to measure the contrast and visualization of structures that do not require a reference image and could be used as cost functions for an optimization problem that seeks the maximization of this information. Some examples of these metrics are the Contrast to Noise Ratio (CNR), Signal to Noise Ratio (SNR), and a classic contrast measure defined by $|\frac{S_1 - S_2}{S_2}|$, where S_1 and S_2 are the mean signal intensities of two different structures.

These methods however require a prior segmentation of the structures being compared, because they take signal intensity differences between different objects of interest. Additionally, they do not take into account perceptual features.

2.3. HVS Sensitivities

In our optimization method we emulate some HVS sensitivities to measure the quality and visual information of images: luminosity and spatial frequency. The variations in sensitivity as a function of luminosity are due to the light-adaptive properties of the retina; and spatial frequency sensitivity is due to the optics of the eye and to features of the nervous system (Daly, 1993). Next we will explain in detail each of these effects.

2.3.1. Luminosity Sensitivity

The sensitivity of the human visual perception to the light that hits the retina is a non linear function, and under certain light conditions it is commonly modeled as a logarithmic function (Daly, 1993).

The sensitivity to intensity differences depends on the local luminance of the image, and according to the Weber-Fechner law, the magnitude of a just-noticeable luminance change ΔL is proportional to the stimulus mean luminance L for background levels above 10 cd/m^2 (Hood & Finkelstein, 1986), under this level the just-noticeable luminance difference increases as luminance decreases.

Chou & Li (1995) stated that two contiguous pixels are visually distinguishable if the gray level difference between them is higher than a threshold. This threshold also depends on local intensities and can be modeled by:

$$f_2(bg(x,y)) = \begin{cases} T_0 \cdot (1 - \sqrt{(bg(x,y)/127)}) + 3 & \text{if } bg \leq 127 \\ \gamma \cdot (bg(x,y) - 127) + 3 & \text{if } bg > 127 \end{cases} \tag{2.1}$$

where bg is the background mean luminance, T_0 and γ represent the visibility threshold when the background grey level is zero, and the curve slope at higher background luminance. Empirically, it has been found that T_0 and is γ are equal to 17 and $\frac{3}{128}$ respectively (Chou & Li, 1995).

As seen in Figure 2.2 the threshold is higher for high and low background luminance levels, whereas its value is smaller for average background levels. This result is consistent with subjective evaluations (Chou & Li, 1995; Hontsch & Karam, 2000; Jayant et al., 1993; Netravali & Haskell, 1988; Safranek & Johnston, 1989).

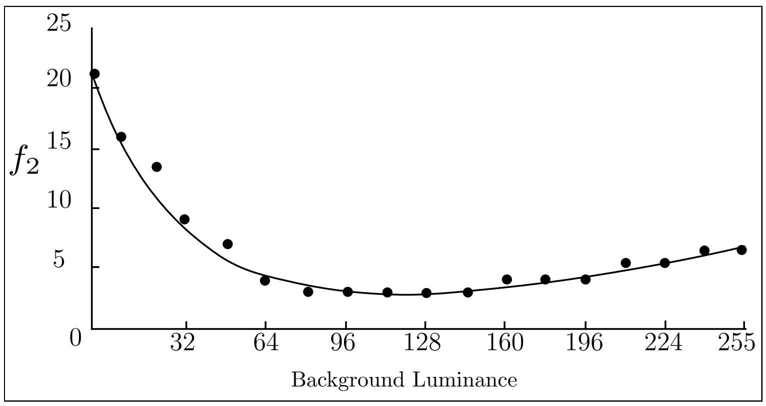

FIGURE 2.2. Visibility thresholds due to background luminance.

2.3.2. Spatial Frequencies

Another interesting HVS property is its sensitivity to spatial changes in light levels. At certain spatial frequencies the HVS is more sensitive to luminosity changes than in others. The Contrast Sensitivity Function (CSF) is defined as the inverse of the Contrast Threshold Function, which is normally defined as the contrast required by an observer to detect waves of a sinusoidal signal of different frequencies. Many CSF models have been proposed, being Mannos & Sakrison (1974) model (Figure 2.3) one of the most accepted:

$$H(u,v) = 2.6(0.0192 + 0.114F_r(u,v)) \cdot exp(-(0.114F_r(u,v))^{1.1}) \tag{2.2}$$

where $F_r(u,v)$ is the normalized image spatial frequency in cycles per degree (cpd). The radial frequency (the rate of change in an orientation angle) is determined by horizontal $f_r(u)$ and vertical $f_r(v)$ frequencies

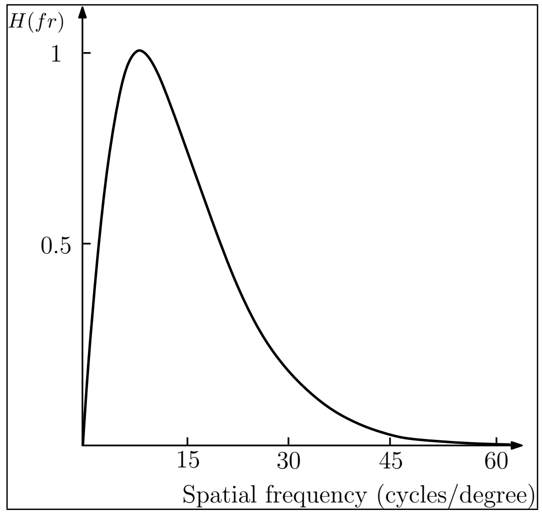

FIGURE 2.3. Contrast Sensitivity Function.

$$f_r(u) = \frac{u-1}{2N\Delta} \quad f_r(v) = \frac{v-1}{2N\Delta} \tag{2.3}$$

where N is the number of points, Δ is the dot pitch (distance between dots of the same color in a screen), and $u, v = 1, 2, ..., N$. The radial frequency is obtained by taking the euclidean distance between these two frequencies - within the frequency domain (Ahumada & Peterson, 1992), which scaled by the viewing distance d is:

$$f_r(u,v) = \frac{\pi}{180 \sin^{-1}\left(\frac{1}{\sqrt{1+d^2}}\right)} \sqrt{f_r(u)^2 + f_r(v)^2} \tag{2.4}$$

Daly (1993) introduced an angular dependent function $S(\Theta(u,v))$ which compensates for viewing angle Θ such that the normalized frequency response is:

$$F_r(u,v) = \frac{f_r(u,v)}{S(\Theta(u,v))} \tag{2.5}$$

with

$$S(\Theta(u,v)) = \frac{1-w}{2}\cos(4\Theta(u,v)) + \frac{1+w}{2} \tag{2.6}$$

where $w = 0.78$ and the angle Θ is defined by:

$$\Theta(u,v) = \tan^{-1}\left(\frac{f_r(u)}{f_r(v)}\right) \tag{2.7}$$

For measuring the quality of images in our optimization method we use these two HVS properties to define a Visibility Map (VM), which allow us to highlight perceptually relevant structures in an image.

These HVS properties are incorporated into our proposed optimization scheme through two different maps: a Relevant Spatial Frequencies (RSF) Map, which aims to distinguish perceptually relevant spatial frequencies in the image; and a Contrast Map that allows recognizing how distinguishable are the pixels in their background. The pixel-by-pixel product between both maps conform the VM, which encodes how visible is each pixel for the HVS.

2.3.3. Relevant Spatial Frequencies Map

To account for the HVS spatial frequency sensitivity, we first apply the two-dimensional discrete cosine transform (DCT) to the entire image with an 8×8 pixel sliding block. We then filter the obtained result using the Mannos & Sakrison (1974) CSF, so that granting a variable importance to the DCT coefficients according to their frequency content. After filtering, we choose the coefficient with the highest absolute value, which is finally placed in the position $(4, 4)$ of the respective block in the image. The entire procedure is shown in Figure 2.4.

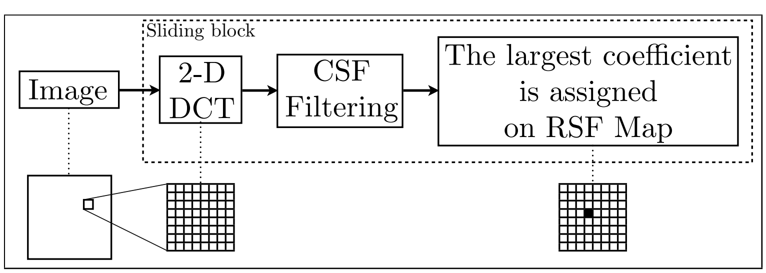

FIGURE 2.4. RSF Map construction procedure.

An example of the RSF map is shown in Figure 2.5(b), which as expected show high values for regions with spatial frequency components around 10 cpd. Since the resulting map is blurred because of the size of the sliding block, we repeat the procedure with a 4×4 block in those cases where the highest coefficient of the 8×8 process corresponded to a frequency greater than 3.5 cpd.

Figure 2.5(c) shows the final RSF map.

2.3.4. Contrast Map

Until now, a pixel visibility due to luminance levels has been defined as a binary variable (visible or not visible) according to a threshold (2.1). We go further and estimate the *probability* of visibility of each pixel in an image. To calculate it, we propose the function $w(\frac{j+n}{2})$ that models the relevance of the difference between the intensity j of a given pixel and the mean intensity n of its eight neighbors (we are using a 3×3 sliding block to define neighborhood).

$$w(\frac{j+n}{2}) = P\left(\mid g_1 - g_2 \mid > f_2\left(\frac{j+n}{2}\right) \middle| \frac{g_1+g_2}{2} = \frac{j+n}{2} \right) \tag{2.8}$$

Assuming that each intensity level is equally probable and a discrete number of intensity levels g_i (e.g. 0 to 255), w can be easily computed off-line for any intensity pair (j, n) if we compute the ratio between the number of intensity pairs (g_1, g_2) that follows the inequity (2.8) and the number of intensity pairs (g_1, g_2) that follows the restriction imposed in the same equation.

For example, Figure 2.6(b) shows three cases, where the difference between a pixel and its background is the same in every case, nevertheless the visual perception is different. In a well calibrated display, it can be noticed that the central pixel in the middle image has better visibility than in the other cases, where the background luminance is

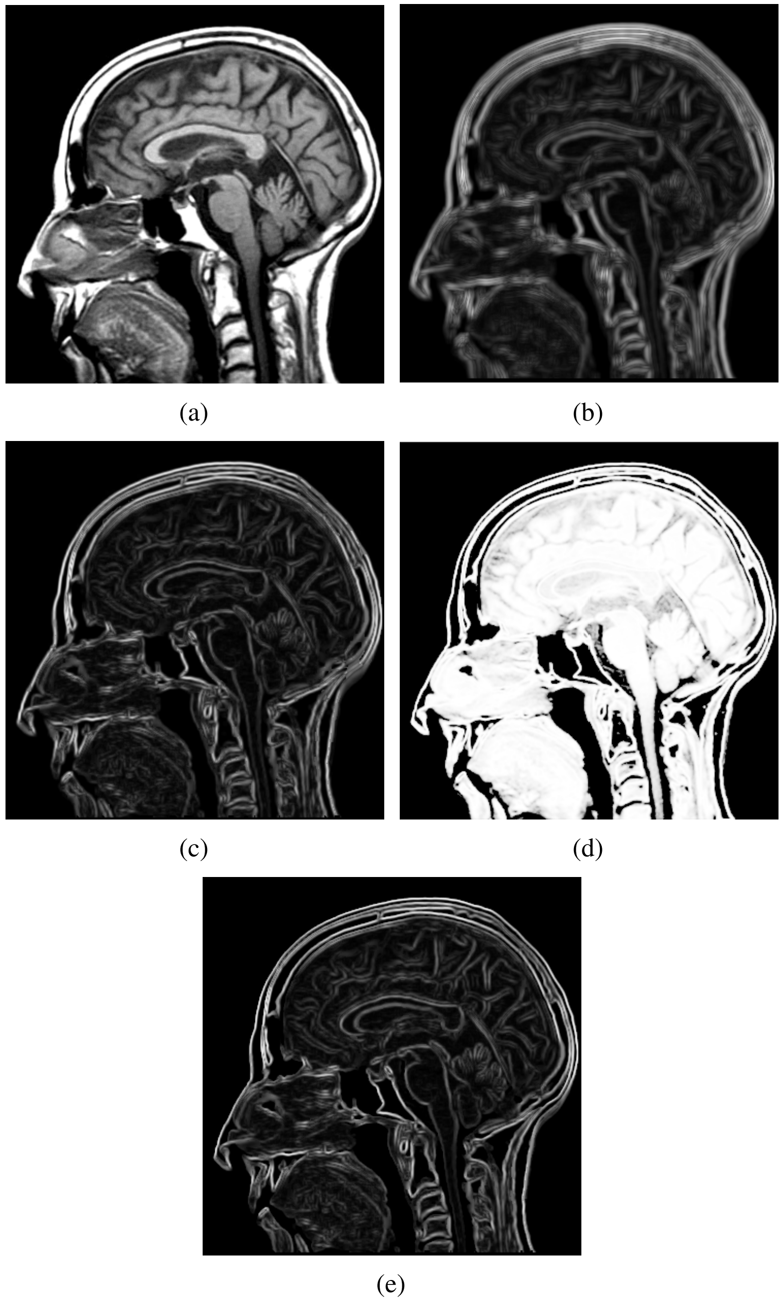

FIGURE 2.5. (a) Original image, (b) RSF Map using 8×8 sliding blocks, (c) RSF Map final, with high frequencies correction using 4×4 sliding blocks, (d) Contrast Map, (e) Visibility Map.

close to the extremes[1]. This result is concordant with function $w(\frac{j+n}{2})$ values, shown in Figure 2.6(a). An example of a Contrast Map is shown in Figure 2.5(d).

[1] In monitors or printed versions well calibrated.

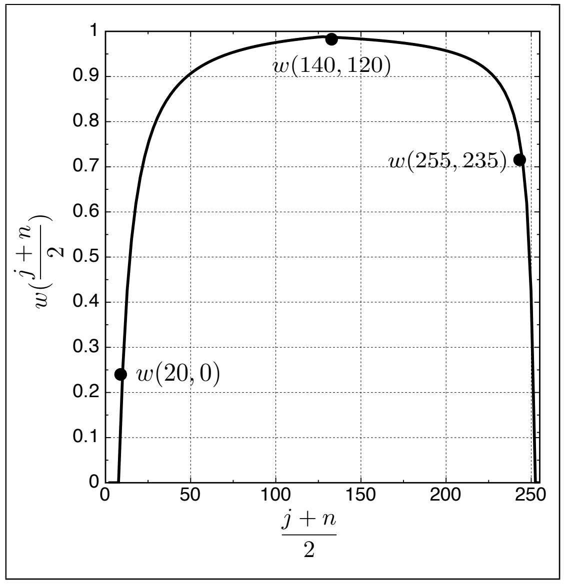

(a)

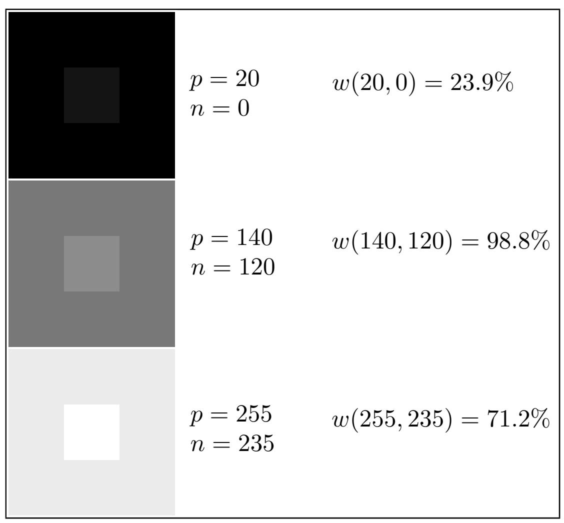

(b)

FIGURE 2.6. (a) Perceptual contrast between a pixel and its background according to their gray levels, (b) $w(\frac{j+n}{2})$ application example.

2.3.5. Visibility Maps

To account for both HVS sensitivities, the Visibility Maps are constructed by taking the pixel-by-pixel product of the two previous maps. So that each pixel in the VM has the contribution of HVS contrast and spatial frequencies sensitivities. In Figure 2.5(e) a VM is presented.

3. VISIBILITY MAPS VALIDATION

Since we are introducing a new index of quality measurement in this section we will compare it with other indices and subjective evaluations.

3.1. Method

To validate the VM as a visual perception measurement, we created a full reference image quality assessment index that is computed directly from a VM. The purpose of this index is to quantify the perceptual similarity between a reference image and a distorted version of it.

Our index is constructed by obtaining the VM for both, a reference image and a distorted image, and then calculate the correlation coefficient between their respective VMs. This index, called *Pixel Visibility Criteria Index* (PVCI), is expressed as:

$$\mathrm{PVCI} = \frac{1}{n-1}\sum_{i=1}^{n}\left(\frac{R_i - \bar{R}}{s_R}\right)\left(\frac{D_i - \bar{D}}{s_D}\right) \tag{3.1}$$

For validating VM and the PVCI as perceptual quality assessment metrics, we use the LIVE database (Sheikh et al., 2005) in which 20-25 subjects were asked to evaluate the quality of pictures according to how visible or annoying were the distortions they had. In the database, 29 high resolution RGB 24-bits/pixel images were used, of a typical size of 768×512 pixels, which were distorted using five types of distortions: JPEG2000, JPEG, white noise in the RGB components, Gaussian blur and transmission errors in the JPEG2000 bit stream using a fast-fading Rayleigh (FF) channel model.

Each of the 29 images were distorted with different levels of distortion of each type, generating images that cover roughly the full range of perceptual qualities. This is a set of 982 images, of which 203 correspond to reference images (the 29 images were displayed seven times each). Observers were asked to provide their perception of quality as “(1) Bad,” “(2) Poor,” “(3) Fair,” “(4) Good,” and “(5) Excellent.”

These values were subtracted for the matching pairs (reference and distorted), were then converted to Z-scores (van Dijk et al., 1995), and finally scaled back to a 1-100 range. This is the difference mean opinion score (DMOS) for each of the distorted images.

Six metrics that cover a wide range of QA methodologies were used as reference: PSNR, MSSIM (Z. Wang et al., 2003), DCTune (Watson, 1993), VSNR (Chandler & Hemami, 2007), VIF (Sheikh & Bovik, 2006) and NQM (Damera-Venkata et al., 2000). Except from DCTune, which we evaluated using the original color images, the rest of the metrics were applied to grayscale versions of the images using the luminance $L = 0.2989R + 0.5870G + 0.1140B$, where R, G and B denote the 8-bit red, green, and blue intensities.

Due to the non-linear relationship between the QA metrics and the visual perception of the images, it is commonly accepted to apply a non-linear fit to the metrics for evaluating their performances. In our case we applied a five parameter function (Sheikh et al., 2006), constrained to be monotonic, so as to obtain the best fit by minimizing the mean squared error:

$$\text{Quality}(x) = \beta_1 \text{logistic}(\beta_2, (x - \beta_3)) + \beta_4 x + \beta_5 \tag{3.2}$$

$$\text{logistic}(\tau, x) = \frac{1}{2} - \frac{1}{1 + exp(\tau x)} \tag{3.3}$$

To assess the performance of PVCI, we use RMSE, Correlation Coefficient (CC) and the Spearman Rank Order Correlation Coefficient (SROCC), which assesses how well the relationship between two variables can be described using a monotonic function.

3.2. Results

We evaluated our quality assessment metric PVCI, assuming a viewing distance of 19.7 inches and a dot pitch of 96 dpi. We calculated the alternative metrics using their implementations available at: (VIF website, 2009; VSNR website, 2009; DCTune website, 2009; SSIM website, 2009; NQM website, 2009).

3.2.1. Performance

PVCI correlates well with observers score using the entire database, with a CC and SROCC close to 88% (Table 3.1). Moreover, if we discard compression distortions PVCI increases its performance more than the other metrics, reaching CC and SROCC values above 95%. This reflects that, unlike the other indexes, PVCI treats differently distortions that are based on local or specific information of the image, from those applied equally across the image.

Figure 3.1 shows the the subjective rating of the perceived distortion (DMOS) against the QA metrics corrected using the logistic function (3.2) for the non-compression-based distortions. As seen, our metric using VM outperforms many of existing QA metrics.

TABLE 3.1. Quality Index performance for entire database and for non-compression-based distorsions, using Correlation Coefficient (CC), Spearman Rank Order Correlation Coefficient (SROCC) and Root Mean Square Error (RMSE). PVCI outperforms the other methods when considering distortions that are not related with compression.

	All data			Noise, blur & FF		
Index	CC	SROCC	RMSE	CC	SROCC	RMSE
PSNR	0.826	0.819	9.097	0.852	0.858	8.410
MSSIM	0.907	0.899	6.788	0.907	0.905	6.762
DCTune	0.778	0.769	10.115	0.790	0.787	9.849
VSNR	0.882	0.889	7.602	0.916	0.926	6.451
VIF	0.948	0.953	5.112	0.968	0.968	4.038
NQM	0.876	0.877	7.756	0.892	0.880	7.269
PVCI	0.885	0.878	7.509	0.953	0.956	4.867

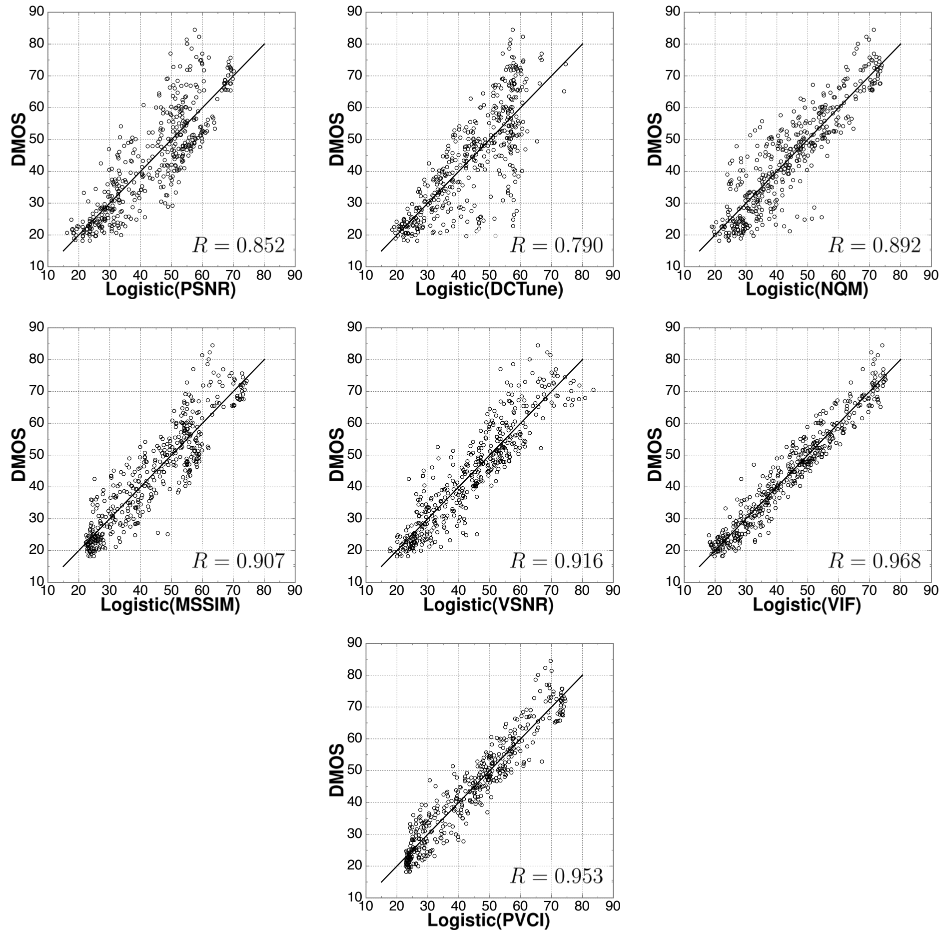

FIGURE 3.1. Subjective scores of perceived distortion for the 319 images without compression of LIVE Sheikh et al. (2005). In all graphs, the horizontal axes correspond to corrected metrics using (3.2). The vertical axes denotes the perceived distortion (DMOS) as reported by subjects.

4. METHODS

4.1. Optimization for MRI

We aim to replicate the procedure done by medical technologists to find optimal acquisition parameters (as shown in Figure 2.1), but analyzing and evaluating the images using a metric based on our VM. This metric is able to incorporate HVS features that make possible the evaluation.

The main idea is to obtain MRIs of the same structure varying the acquisition parameters, and by using an index to quantify and optimize the perceptual information provided by each set of paremeters. Thus, to obtain the optimal parameter configuration for the patient (as shown in Figure 4.1).

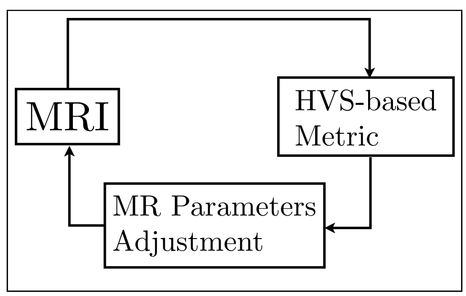

FIGURE 4.1. MRI parameters setting using HVS-based metric.

4.2. Optimization Cost Function

VM allow quantifying the perceptually relevant information in any region of an image. This information can be used as the objective function for an optimization problem that maximizes the *Region Visibility Information* (RVI) (i.e. the visibility of a desired region or structure) by changing the acquisition parameters.

Our method consists on using the VM of the region of interest to optimize the acquisition parameters p. Our cost function will be the standard deviation of the VM for that given region.

$$\max_{p} \text{ RVI} = \sigma\left(\text{VM}(\mathbf{I}(m,p)|_{\Omega})\right) \tag{4.1}$$

where $\mathbf{I}$ is the MR scan obtained of a region m.

We use the standard deviation of the VM in ROI, because it captures the dispersion of existing visibility, which is higher in areas with high structural content, such as edges or textured areas.

4.3. Implementation

To find optimal acquisition parameters, we propose the following scheme: (1) acquire a few scans using different values of the acquisition parameters in an expected optimal range. (2) Define a ROI which covers roughly a portion of the object of interest and its background. (3) Calculate the RVI index in each of the images within the ROI. (4) Interpolate the RVI index to obtain the visibility of structures for those values in the range that were not evaluated. We are assuming that the RVI index gives a smooth continuous function, condition that we effectively verified (vide infra).

4.4. Subjective Experiments for Validation

We considered two frequent applications in MRI to assess our optimization method. The first one was to find the parameters needed to enhance white matter (WM) in the brain while suppressing Gray Matter (GM) and cerebrospinal fluid (CSF). The second one was to find the parameters needed to differentiate WM from GM making visible both tissues.

For the first case we consider an Inversion Recovery (IR) sequence with Time of Inversion (T_I) and Time of Echo (T_E) as the optimization variables, and for the second one a Spin Echo (SE) sequence with Time of Repetition (T_R) and T_E as the optimization variables.

4.4.1. Optimal Range Selection

The optimization parameters should cover roughly the expected optimal range. To find this range we use the signal equation for a IR sequence:

$$s = M_0 \cdot (1 - 2e^{-T_I/T_1} + e^{-T_R/T_1})e^{-T_E/T_2} \tag{4.2}$$

where $T_1 = 780$ ms and $T_2 = 90$ ms for WM, $T_1 = 920$ ms and $T_2 = 100$ ms for GM and $T_1 = 3000$ ms and $T_2 = 1420$ ms for CSF for a 1.5 T magnetic field (Chary & Govil, 2008). Normalizing M_0 to 100, setting a sufficiently long T_R to 1200 ms and choosing the minimum allowable $T_E \approx 10$ ms, one can plot the signal intensity against T_I (Figure 4.2).

It can be seen that bellow $T_I \approx 400$ ms the contrast is reversed in the images, therefore it is interesting to use T_I values greater than 400 ms.

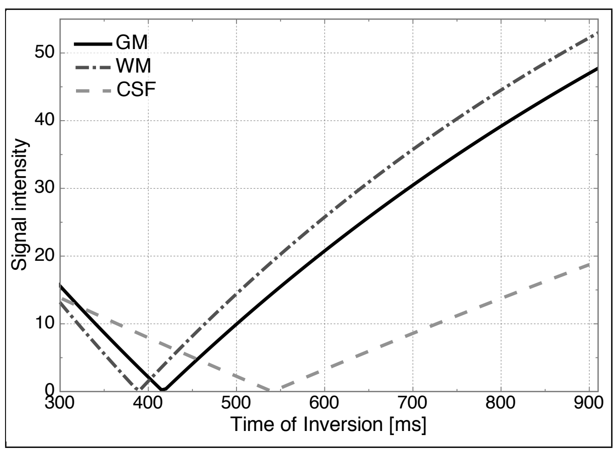

FIGURE 4.2. Plot of the theoretical WM, GM and CSF signals (in magnitude) as a function of Time of Inversion for an IR sequence with $M_0 = 100$, $T_R = 1200$ ms and $T_E = 10$ ms.

To have a margin of error and to cover a wide range of values, the chosen T_I ranged from 375 ms to 750 ms, with a higher sampling rate in values close to 400 ms. This way, T_I was set at: 375 ms, 400 ms, 450 ms, 500 ms, 600 ms and 750 ms. For choosing T_E, we simply covered a wide range of values starting from the minimum. This way we set T_E to 10 ms, 25 ms and 40 ms, resulting eighteen MR scans (Figure 4.3).

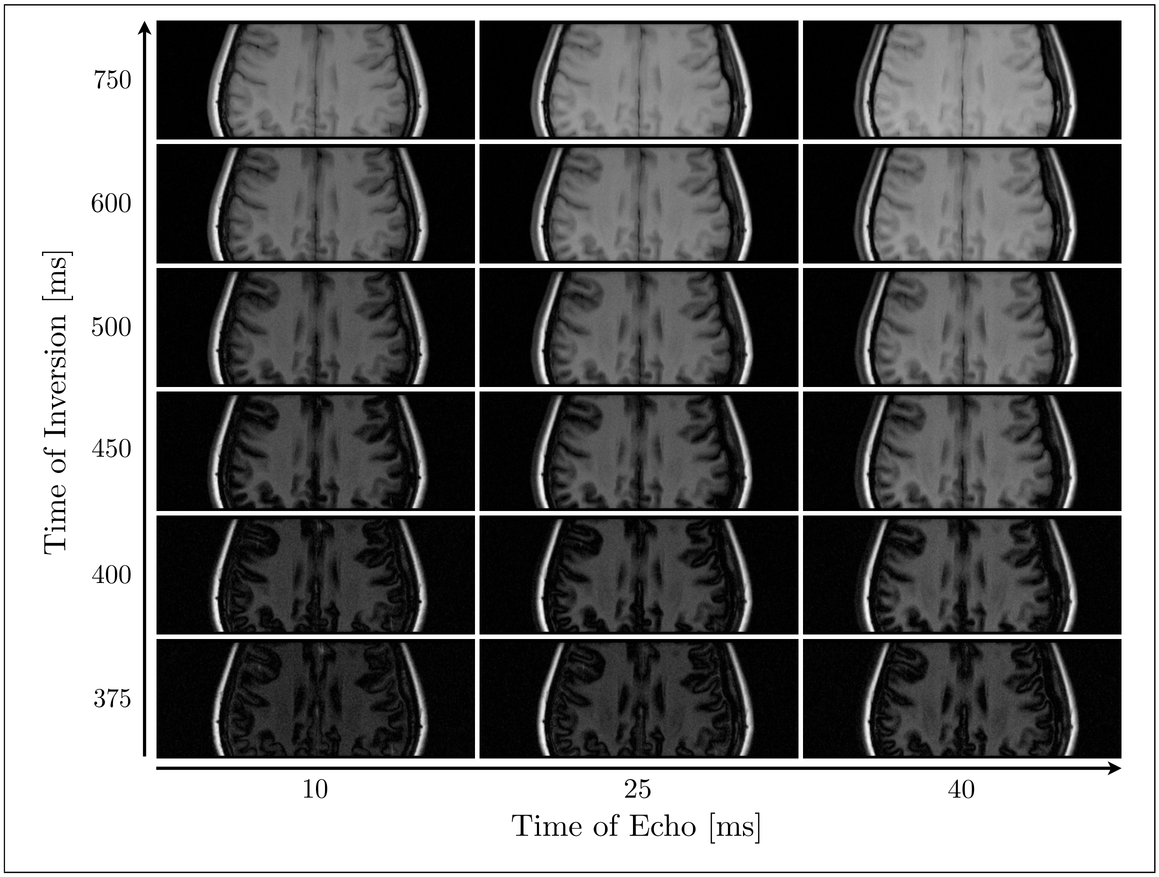

FIGURE 4.3. IR scans obtained within the expected optimal range for the WM visibility optimization and GM and CSF suppression.

For the Spin Echo sequence we acquired sixteen scans shown in Fig 4.4, using T_E: 4.0 ms, 4.3 ms, 4.6 ms, and 4.9 ms; and T_R: 10 ms, 15 ms, 20 ms and 25 ms.

4.4.2. RVI Index Evaluation

The first step for evaluating our perceptual index is to select a ROI where the structures of interest are located, in our case a region with WM, GM and CSF. It is not important to be precise in selecting the ROI, however it is desirable to avoid including undesired structures which may influence the calculation of the index (e.g. bone or fat).

Our HVS-based metric RVI is then evaluated on the acquired MRI scans, in order to quantify the perceptually relevant information in the selected ROI of each image. We interpolate these results with a triangle-based cubic method using the griddata MATLAB

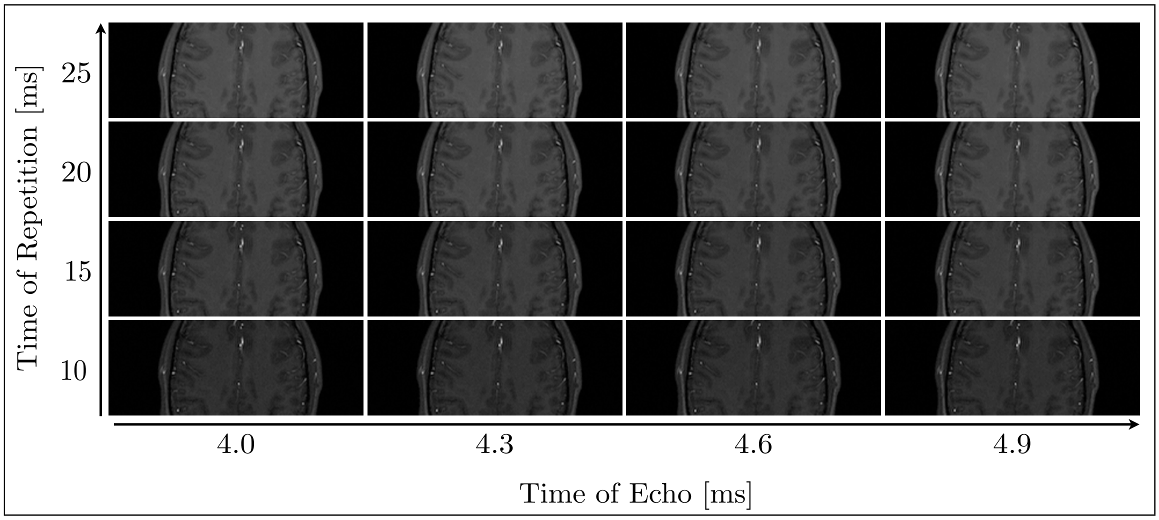

FIGURE 4.4. SE scans obtained for the differentiation between GM and WM.

function (The MathWorks, Natick 2008), so that to estimate the RVI for those values in the range that were not sampled.

For validation purposes, ten healthy volunteers (seven men and three women; mean age, 24 years; range 22–27 years) were scanned with the IR sequence explained above. For the SE sequence, we scanned six healthy volunteers (five men and one woman; mean age, 26 years; range 24–33 years) with the described sixteen T_E/T_R combinations.

In order to verify whether or not our RVI is a smooth and continuous function that can be well approximated by a cubic interpolation, we performed five additional scans to one volunteer using additional T_I/T_E combinations within the range (Figure 4.5). This way we compared the RVI index obtained directly from the scans with those obtained from the interpolations, in order to evaluate whether the computed optimum corresponded to the visual optimal using the optimal parameters obtained through the optimization process. The additional scans were acquired using the following $(T_E, T_I) = (30, 412)$, $(18, 425)$, $(33, 475)$, $(33, 550)$, $(18, 675)$ ms.

The IR scans were acquired with a field of view of 220×220 cm and an acquisition matrix of 312×312 pixels yielded to an in-plane resolution of 7×7 mm. For the SE scans we considered a field of view of 220×220 cm and an acquisition matrix of 240×240

pixels, resulting in a 9×9 mm resolution. In order to shorten acquisition time, we reduced the FOV by 50% using Regional Saturation Bands (REST Slabs) in the phase encoding direction.

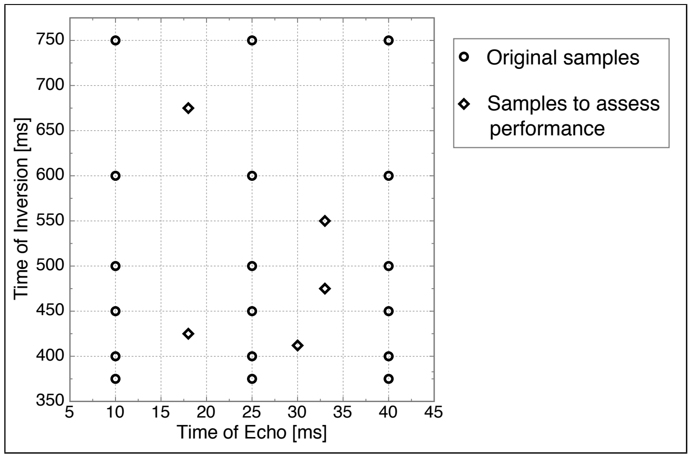

FIGURE 4.5. Expected optimal range with original samples (○) and samples used to asess the performance of the interpolation needed for the RVI computation (◇).

4.4.3. Subjective Experiment

In order to validate the results of our perceptual metric, nine radiology residents (four of them in their second year and five on their third year), a radiologist and two medical technologists were asked to rate the scans according to how well did they meet the objective in each case. We use a continuous linear scale that was divided into five levels.

The observer scores were converted to a 1 to 5 scale, where 1 corresponds to “Bad”, 2 is “Poor”, 3 is “Fair”, 4 is “Good” and 5 “Excellent”.

We compared this mean opinion score (MOS) with the values obtained by our RVI index using three criteria: computing the correlation coefficient between RVI scores and MOS of the images; computing the interpolation errors between interpolated and calculated RVI values; and measuring the accuracy of RVI to find the optimal parameters within the chosen range, using as benchmark a contrast-based optimization. We calculated the cost function of this alternative method, by computing the average intensity of each tissue of interest, which we previously manually segmented. And then we took the subtraction between both tissues intensities, and divided it into the mean intensity of one of them.

5. RESULTS

5.1. Correlation Between RVI and MOS

As shown in Tables 5.1 and 5.2, the correlation coefficient for the IR sequence is above 0.8 in every case, while for the SE sequence, the correlation coefficient ranged between 0.515 and 0.744.

In the SE sequence, the CC between MOS and RVI index for volunteers 5 and 6 image sets are lower than for the rest of the volunteers (Table 5.2) because their images have some differences with the others. For instance, the average MOS in volunteer 5 image set is 2.53, while for the rest is 3.50 (standard deviation 0.03), which means the observers could not clearly distinguish WM from GM in that set. And in volunteer 6 image set, observers found it difficult to appreciate differences between the images, which is reflected in the lower deviation of MOS (0.258) compared with the rest of image sets (0.405 mean deviation) (Table 5.2).

TABLE 5.1. Correlation coefficient between subjective scores and RVI index, and optimal T_E, T_I parameters obtained by RVI optimization, Contrast optimization and Observer scores for the eighteen IR scans.

	CC	RVI Opt. (T_E,T_I)	Contrast Opt. (T_E,T_I)	MOS Opt. (T_E,T_I)
Volunteer 1	0.9233	(27,405)	(40,375)	(25,413)
Volunteer 2	0.9004	(40,375)	(21,375)	(40,390)
Volunteer 3	0.9103	(40,398)	(24,405)	(35,413)
Volunteer 4	0.8431	(40,398)	(22,398)	(37,398)
Volunteer 5	0.8281	(27,405)	(10,405)	(26,412)
Volunteer 6	0.8775	(30,413)	(10,398)	(40,405)
Volunteer 7	0.9248	(40,398)	(24,405)	(40,420)
Volunteer 8	0.8060	(40,405)	(12,428)	(40,413)
Volunteer 9	0.8388	(40,398)	(10,398)	(38,405)
Volunteer 10	0.8628	(28,443)	(27,405)	(28,450)

As shown in Figure 5.1, for the IR sequences the cost functions obtained with the RVI index (Figure 5.1(b)) is similar to the MOS evaluations (Figure 5.1(a)). It can be seen that both surfaces show that the WM visibility decreases when T_I increases over 450

TABLE 5.2. Correlation coefficient between subjective scores and RVI index, and optimal T_E, T_R parameters obtained by the RVI optimization, Contrast optimization and Observer scores for the sixteen SE scans.

	CC	RVI Opt. (T_E,T_R)	Contrast Opt. (T_E,T_R)	MOS Opt. (T_E,T_R)	MOS (μ, σ)
Volunteer 1	0.7420	(4.578,25)	(4.000,10.0)	(4.578,21.1)	(3.50,0.34)
Volunteer 2	0.7241	(4.617,25)	(4.617,10.0)	(4.477,23.1)	(3.49,0.42)
Volunteer 3	0.7261	(4.000,25)	(4.298,10.0)	(4.000,25.0)	(3.52,0.36)
Volunteer 4	0.7444	(4.558,25)	(4.598,13.8)	(4.298,25.0)	(3.47,0.49)
Volunteer 5	0.5554	(4.898,25)	(4.598,15.7)	(4.618,25.0)	(2.53,0.41)
Volunteer 6	0.5151	(4.898,25)	(4.898,14.4)	(4.000,24.8)	(3.55,0.26)

ms. Additionally, both metrics show that for low T_E and T_I values, WM visibility is very low.

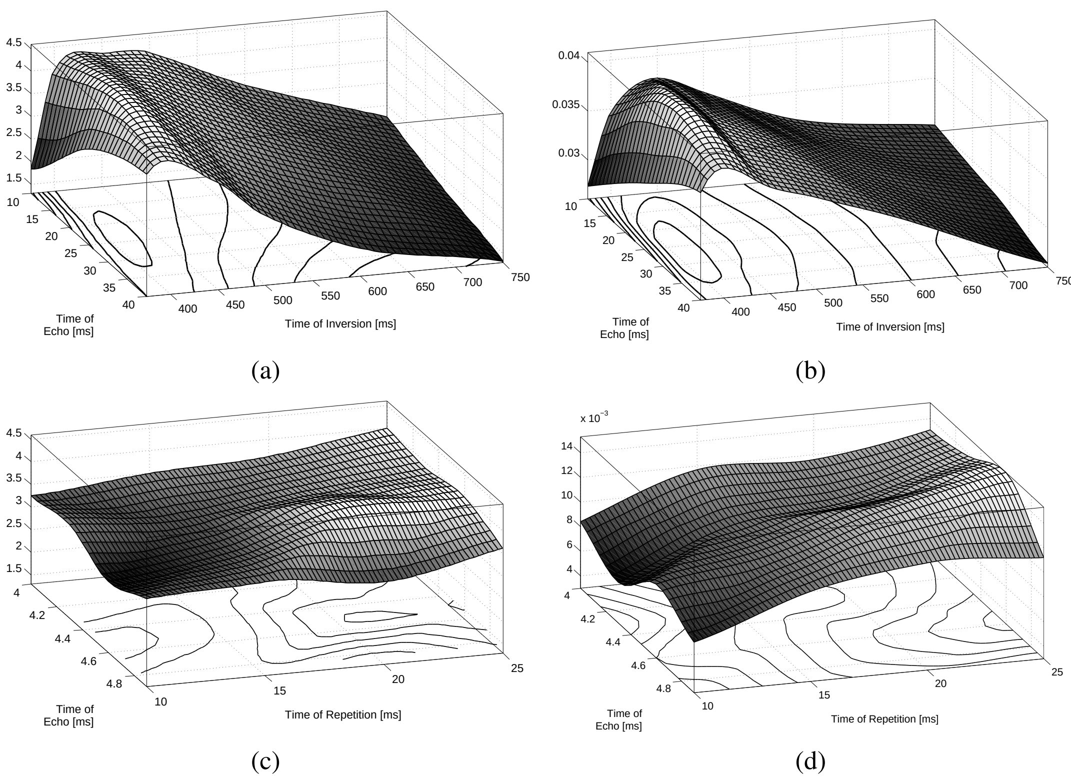

FIGURE 5.1. Objective function from volunteer 1 for the IR sequence parameters optimization using (a) MOS, and (b) RVI metric. And for the SE sequence using (c) MOS, and (d) RVI.

5.2. Interpolation Errors

As seen in Figure 5.2, the differences between interpolated and calculated RVI values were never higher than 5.76%, value reached at the (T_E, T_I) pair equal to $(33, 550)$ ms, where the interpolated value for RVI is 0.451 and the calculated one is 0.425. Nevertheless, for this acquisition parameter configuration the visibility of WM is low (MOS $= 2.00$) so its effect on the optimization result is negligible. The second higher difference is at $(18, 425)$ ms with a 5.19%, where 0.0475 and 0.0501 are the values for calculated and interpolated RVI, respectively. For the rest of the pairs $(30, 412)$, $(33, 475)$ and $(18, 675)$ ms, the difference is 3.25%, 2.88% and 1.12%, respectively.

The correlation coefficient between MOS and RVI index did not suffer a significant variation when we replaced the five additional measured values (CC = 0.8456) with interpolated values (CC = 0.8377).

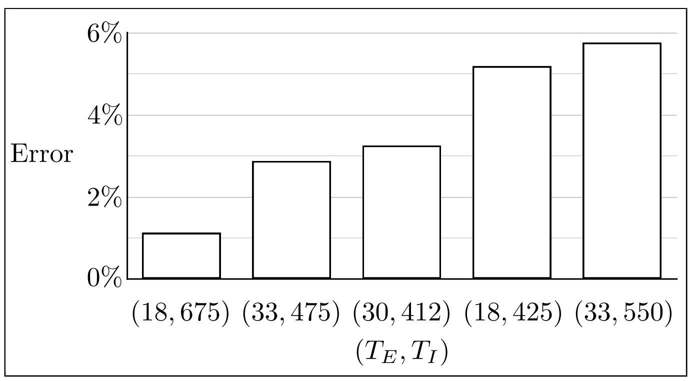

FIGURE 5.2. Percentage error between interpolated and calculated RVI for additional scans.

5.3. Accuracy in Locating the Optimum

To assess the accuracy in locating the optimal parameters, we compare the optima found by RVI and by the observers, using the interpolation method in both cases.

Tables 5.1 and 5.2 show the optimal parameters obtained using our perceptual metric RVI, the classic contrast measure calculated for GM and WM signals and MOS. It can be seen for the IR sequence that the difference between the optimal T_E obtained by RVI and

MOS is never higher than 10 ms (mean 2.3 ms, 7.7% error), and 22 ms (mean 9.7 ms, 2.6% error) in the case of T_I. For the SE sequence, the highest difference between both scores is 0.9 ms for T_E (mean 0.263 ms, 26% error) and 3.86 ms (mean 0.997 ms, 6.6% error) for T_R.

We calculated and plotted the difference between the ideal optimal parameters (using MOS) and RVI optimal parameters, and by MOS and the contrast method (Figure 5.3). In the coordinate system, the pair (x, y) indicates that the difference of T_E between the optimization method and MOS is in the x axis, and the difference of T_I (or T_R in SE sequence) is in the y axis.

In the last experiment, the best rated images (MOS rate) were the ones that we obtained using the parameters defined by the RVI-based optimization.

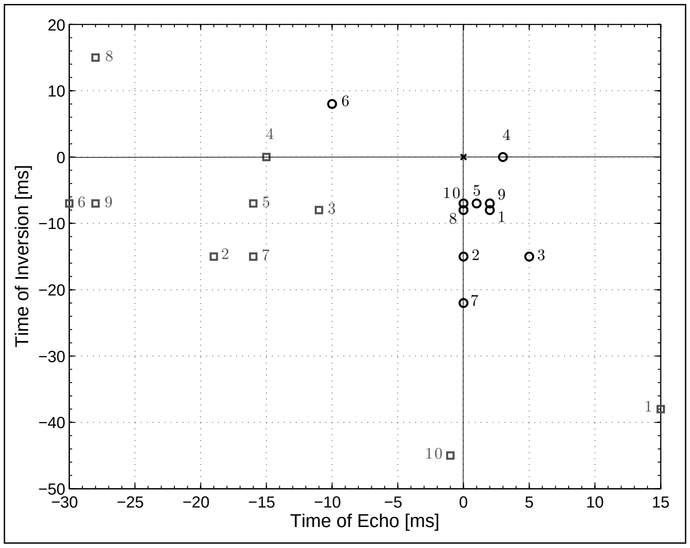

(a) IR Sequence

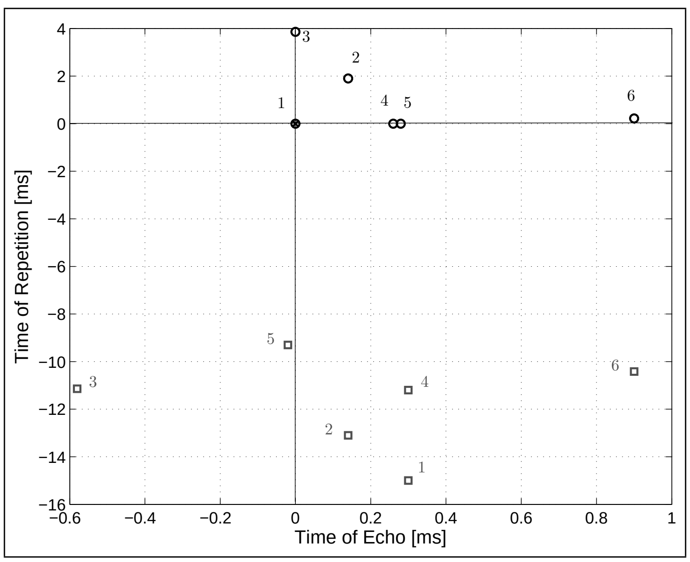

(b) SE Sequence

FIGURE 5.3. Difference between the optimal parameters found by observers and RVI (○), and by observers and the contrast method (□). Attached to every point is a number that indicates the correspondent volunteer.

6. DISCUSSION

6.1. Visibility Maps Validation Method

Our QA methodology, like JPEG compression, works on a block-by-block basis. This is the reason why when assessing quality for compressed images PVCI does not encompass all its dynamic range (between 0 and 1), as it occurs for the rest of distortions which are applied equally throughout the images.

It is also interesting to appreciate the performance of VM applied to QA when there is no compression on images, because VM are intended to be used in medical imaging, in which lossy compression methods such as JPEG or JPEG 2000 are avoided. As can be seen in Figure 3.1, our metric has a good correlation with human perception of these distortions, outperforming many of the existing FR QA methods, which means that VM can properly assess the visual information contained in images.

6.2. Acquisition Parameters Optimization

In our case, the expected optimal range for the IR sequence could be smaller, because the optimum T_I for every volunteer is close to 400 ms, while the sampling was done with values up to 750 ms. So it is possible to optimize with less samples using values below 500 ms, i.e. removing the acquisitions with $T_I = 600$ and 750 ms. This way, the optimization can be performed with only twelve acquisitions, which implies shorter acquisition time.

In the SE sequence optimization, the accuracy locating the optimal T_R is better than locating the optimal T_E, because the contrast depends more on the first parameter. As can be seen in Table 5.2, the subjective optimal T_R is above 21 ms in every case, which implies that the optimum is always found in the top 27% of the range (i.e observers always show preference for higher T_R), while the optimal T_E ranges between 4.0 ms and 4.618 ms, covering the 69% of the range.

7. CONCLUSION

We have proposed a HVS-based method which allows to perform applications in the field of medical imaging, such as MRI acquisition parameters optimization. The method makes use of two HVS features: its sensitivity to luminosity and spatial frequencies, which are reflected in perceptual maps named Visibility Maps.

For MRI acquisition parameters optimization we proposed a method to maximize the visibility of a desired structure in a scan. We tested the method for two common MRI applications: the white matter visibility maximization, using an IR sequence, and the contrast enhancement between gray matter and white matter using a SE sequence. The methods were based on searching the optimal T_E and T_I, and T_E and T_R parameters respectively, by acquiring some scans within an expected optimal range.

The results of the optimization show that the method based on VM can successfully find optimal parameters for these specific tasks and can also maximize the visibility of other tissues without the need of previous segmentation of the scans.

The validation of VM as a perceptual quality metric, using it for Full Reference Image Quality Assessment, shows that our method can properly measure the visibility of each pixel of an image according to the HVS. Indeed, the comparison between images is not performed between gray levels, but in terms of perceptual information.

As future work, the optimization method can be used to maximize the visibility of other structures in MRI scans, where the acquisition parameters are difficult to set.

References

Ahumada, A. J., & Peterson, H. A. (1992, August). Luminance-model-based DCT quantization for color image compression. In B. E. Rogowitz (Ed.), *Society of photo-optical instrumentation engineers (spie) conference series* (Vol. 1666, p. 365-374).

Alger, J. R., Harreld, J. H., Chen, S., Mintorovitch, J., & Lu, D. (2001, Nov.). Time-to-echo optimization for spin echo magnetic resonance imaging of liver metastasis using superparamagnetic iron oxide particles. *Journal of Magnetic Resonance Imaging*, *14*(5), 586–594.

Avcibas, I., Sankur, B., & Sayood, K. (2002). Statistical Evaluation of Image Quality Measures. *Journal of Electronic Imaging*, *11*, 206–223.

Bradley, A. (1999, May). A wavelet visible difference predictor. *Image Processing, IEEE Transactions on*, *8*(5), 717-730.

Breitmeyer, B. G., & Ogmen, H. (2006). *Visual Masking: Time Slices through Conscious and Unconscious Vision* (2nd ed ed.). Oxford University Press: Oxford.

Carevic, D., & Caelli, T. (1997). Region based coding of color images using KLT. *Graphical Models and Image Processing*, *59*(1), 27-38.

Chandler, D. M., & Hemami, S. S. (2007, Sept.). VSNR: A Wavelet-Based Visual Signal-to-Noise Ratio for Natural Images. *Image Processing, IEEE Transactions on*, *16*(9), 2284-2298.

Chang, L.-W., Wang, C.-Y., & Lee, S.-M. (1999). Designing jpeg quantization tables based on human visual system. In *Image processing, 1999. icip 99. proceedings. 1999 international conference on* (Vol. 2, p. 376-380 vol.2).

Chary, K., & Govil, G. (2008). *NMR in Biological Systems: From Molecules to Human* (1st ed ed.). Springer.

Chen, G.-H., Yang, C.-L., Po, L.-M., & Xie, S.-L. (2006, May). Edge-Based Structural Similarity for Image Quality Assessment. In *Acoustics, speech and signal processing, 2006. icassp 2006 proceedings. 2006 ieee international conference on* (Vol. 2, p. II-II).

Chou, C.-H., & Li, Y.-C. (1995, Dec). A perceptually tuned subband image coder based on the measure of just-noticeable-distortion profile. *Circuits and Systems for Video Technology, IEEE Transactions on*, *5*(6), 467-476.

Czekanowski, J. (1913). Zarys metod statystycznych w zastosowaniu do anthropolgii. *Towarzystwo Naukowe Warszawskie*.

Daly, S. (1993). The visible differences predictor: an algorithm for the assessment of image fidelity. In *Digital images and human vision* (pp. 179–206). Cambridge, MA, USA: MIT Press.

Damera-Venkata, N., Kite, T. D., Geisler, W. S., Evans, B. L., & Bovik, A. C. (2000, Apr). Image quality assessment based on a degradation model. *Image Processing, IEEE Transactions on*, *9*(4), 636-650.

DCTune website. (2009). http://vision.arc.nasa.gov/dctune/.

Dousset, M., & al. et. (1989, Jan.). Short TI Inversion-Recovery Imaging of the Liver: Pulse-Sequence Optimization and Comparison with Spin-Echo Imaging. *Radiology*, *171*(2), 327–333.

Hasan, K. M., Parker, D. L., & L., A. A. (2002, June). Magnetic resonance water self-diffusion tensor encoding optimization methods for full brain acquisition. *Image Analysis and Stereology*, *21*(2), 87–96.

Hontsch, I., & Karam, L. J. (2000, Sep). Locally adaptive perceptual image coding. *Image Processing, IEEE Transactions on*, *9*(9), 1472-1483.

Hood, D. C., & Finkelstein, M. A. (1986). The visible differences predictor: an algorithm for the assessment of image fidelity. In K. Boff, L. Kaufman, & J. Thomas (Eds.), *Handbook of perception and visual performance, volume 1: Sensory processes and perception* (pp. 5.1–5.66). NY, USA: John Wiley and Sons.

Hsiao, W. H., Ip, E., & Millane, R. P. (2003, Nov.). Effects of spectral amplitude and phase errors on interpretability of images. In *Proc. image and vision computing* (p. 175-180).

Jayant, N., Johnston, J., & Safranek, R. (1993, Oct). Signal compression based on models of human perception. *Proceedings of the IEEE*, *81*(10), 1385-1422.

Jones, D. K., Horsfield, M. A., & Simmons, A. (1999, September). Optimal strategies for measuring diffusion in anisotropic systems by magnetic resonance imaging. *Magn Reson Med*, *42*(3), 515–525.

Kim, M.-J., Kim, J. H., Choi, J. Y., Park, S. H., Chung, J.-J., Kim, K. W., et al.(2006). Optimal TE for SPIO-Enhanced Gradient-Recalled Echo MRI for the Detection of Focal Hepatic Lesions. *American Journal of Roentgenology*, *187*(3), W255-266.

Lee, J. W., Kim, J. H., Kang, H. S., Lee, J. S., Choi, J.-Y., Yeom, J.-S., et al. (2006, July). Optimization of Acquisition Parameters of Diffusion-Tensor Magnetic Resonance Imaging in the Spinal Cord. *Investigative Radiology*, *41*(7), 553–559.

Mannos, J., & Sakrison, D. (1974, Jul). The effects of a visual fidelity criterion of the encoding of images. *Information Theory, IEEE Transactions on*, *20*(4), 525-536.

Netravali, A. N., & Haskell, B. (1988). *Digital Pictures: Representation and Compression*. Plenum Press.

NQM website.(2009). http://signal.ece.utexas.edu/software/. (Refer to the nqm.m MATLAB function included in the image quality 1.0 archive)

Papadakis, N. G., Xing, D., Huang, C. L. H., Hall, L. D., & Carpenter, T. A. (1999, March). A comparative study of acquisition schemes for diffusion tensor imaging using MRI. *Journal of Magnetic Resonance*, *137*(1), 67–82.

Peng, H., & Arfanakis, K.(2007, February). Diffusion tensor encoding schemes optimized for white matter fibers with selected orientations. *Magnetic Resonance Imaging*, *25*(2), 147–153.

Ponomarenko, N., Battisti, F., Egiazarian, K., Astola, J., & Lukin, V.(2009, Jan.). Metrics performance comparison for color image database. In *Fourth international workshop on video processing and quality metrics for consumer electronics.*

Pratt, W. K.(1978). *Digital image processing*. NY, USA: Wiley.

Safranek, R. J., & Johnston, J. D.(1989). A perceptually tuned subband image coder with image dependent quantization and post-quantization data compression. In *Proc. ieee int. conf. acoust., speech, and signal processing* (Vol. 3, pp. 1945–1948).

Sheikh, H. R., & Bovik, A. C. (2006, Feb.). Image information and visual quality. *Image Processing, IEEE Transactions on*, *15*(2), 430-444.

Sheikh, H. R., Sabir, M. F., & Bovik, A. C. (2006, Nov.). A Statistical Evaluation of Recent Full Reference Image Quality Assessment Algorithms. *Image Processing, IEEE Transactions on*, *15*(11), 3440-3451.

Sheikh, H. R., Wang, Z., Cormack, L., & Bovik, A. C. (2005). *LIVE Image Quality Assessment Database Release 2.* http://live.ece.utexas.edu/research/quality.

Skare, S., Hedehus, M., Moseley, M. E., & Li, T. Q. (2000, December). Condition number as a measure of noise performance of diffusion tensor data acquisition schemes with MRI. *Journal of Magnetic Resonance*, *147*(2), 340–352.

Spearman, C. (1987). The proof and measurement of association between two things. *The American Journal of Psychology*, *100*(3/4), 441–471.

SSIM website. (2009). http://www.ece.uwaterloo.ca/~z70wang/research/ssim/.

van Dijk, A. M., Martens, J.-B., & Watson, A. B. (1995, February). Quality asessment of coded images using numerical category scaling. In N. Ohta, H. U. Lemke, & J. C. Lehureau (Ed.), *Society of photo-optical instrumentation engineers (spie) conference series* (Vol. 2451, p. 90-101).

Vidarsson, L., Conolly, S. M., Lim, K. O., Gold, G. E., & Pauly, J. M. (2005). Echo time optimization for linear combination myelin imaging. *Magnetic Resonance in Medicine*, *53*(2), 398–407.

VIF website. (2009). http://live.ece.utexas.edu/research/quality/VIF.htm.

VSNR website. (2009). http://foulard.ece.cornell.edu/dmc27/vsnr/vsnr.html.

Wang, B., Wang, Z., Liao, Y., & Lin, X. (2008, Oct.). HVS-based structural similarity for image quality assessment. In *Signal processing, 2008. icsp 2008. 9th international conference on* (p. 1194-1197).

Wang, Z., & Bovik, A. (2009, Jan.). Mean squared error: Love it or leave it? a new look at signal fidelity measures. *Signal Processing Magazine, IEEE*, *26*(1), 98-117.

Wang, Z., & Bovik, A. C. (2002, Mar). A universal image quality index. *Signal Processing Letters, IEEE*, *9*(3), 81-84.

Wang, Z., Bovik, A. C., & Lu, L. (2002). Why is image quality assessment so difficult? In *Acoustics, speech, and signal processing, 2002. proceedings. (icassp '02). ieee international conference on* (Vol. 4, p. IV-3313-IV-3316 vol.4).

Wang, Z., Bovik, A. C., Sheikh, H. R., & Simoncelli, E. P. (2004, April). Image quality assessment: from error visibility to structural similarity. *Image Processing, IEEE Transactions on*, *13*(4), 600-612.

Wang, Z., Simoncelli, E. P., & Bovik, A. C. (2003, Nov.). Multiscale structural similarity for image quality assessment. In *Signals, systems and computers, 2003. conference record of the thirty-seventh asilomar conference on* (Vol. 2, p. 1398-1402 Vol.2).

Watson, A. B. (1993). DCTune: A technique for visual optimization of DCT quantization matrices for individual images. In *Society for information display digest of technical papers* (Vol. XXIV, pp. 946–949).

Yang, C.-L., Gao, W.-R., & Po, L.-M. (2008, Oct.). Discrete wavelet transform-based structural similarity for image quality assessment. In *Image processing, 2008. icip 2008. 15th ieee international conference on* (p. 377-380).

Zhang, X. H., Lin, W. S., & Xue, P. (2005). Improved estimation for just-noticeable visual distortion. *Signal Process.*, *85*(4), 795–808.